Available online at www.sciencedirect.com
ScienceDirect
Acta Materialia 57 (2009) 3367–3373
Acta MATERIALIA
www.elsevier.com/locate/actamat

Interaction between the Kirkendall effect and the inverse Kirkendall effect in nanoscale particles

A.M. Gusak [a,*], K.N. Tu [b]

[a] Department of Physics, Cherkasy National University, 18031 Cherkasy, Ukraine
[b] Department of Materials Science and Engineering, University of California at Los Angeles, Los Angeles, CA 90095-1595, USA

Received 15 August 2008; received in revised form 22 March 2009; accepted 29 March 2009
Available online 4 May 2009

Abstract

A simple kinetic model of the interaction between the Kirkendall effect and the inverse Kirkendall effect in hollow nano-shell formation by solid-state reaction is presented. The difference in vacancy concentrations at the inter-phase boundaries (and corresponding vacancy gradients) is taken into account as well as the curvature effect on the driving force of the reaction. A criterion for nano-shell formation is proposed.

Keywords: Diffusion; Nanostructure; Vacancies; Voids; Reaction

1. Introduction

The classic Kirkendall effect of interdiffusion in a diffusion couple of A and B [1] showed that, when the flux of A is not equal to the flux of B, a vacancy flux will be generated to balance the interdiffusion. Darken [2] provided a kinetic analysis of the effect and included marker motion. An implicit assumption used in the analysis is that vacancy distribution in the diffusion couple is equilibrium everywhere. In other words, the sources and sinks of vacancy are fully operative everywhere in the sample, for example, by dislocation climb. On the basis of this assumption, there are three important implications. First, a lattice shift or Kirkendall shift occurs which can be measured by marker motion. Second, because of the lattice shift, no stress is generated. Third, because equilibrium vacancy is assumed, there cannot be super-saturated vacancies, so no nucleation of void and, in turn, no void formation can take place. However, in actual diffusion couples, the vacancy sources and sinks are often partially effective, and voids have been found and bending of the sample has occurred due to stress, especially in the interdiffusion between a metal thin film and a Si wafer. The voids are sometimes called Frenkel voids rather than Kirkendall voids [3]. Strictly speaking, under the assumption of Kirkendall shift, there should be no Kirkendall voids. But experimentally, they can coexist, so one can have two competing Kirkendall effects: Kirkendall shift and Kirkendall voiding [3–5]. Both are caused by divergence of vacancy flux generated by the difference in intrinsic fluxes of the main components. It is known that, by using hydrostatic compression, void formation can be suppressed, and lattice shift can be recovered [3]. However, in nanosystems, where there is little space for dislocations, and shift in spherical samples may lead to large stresses, Kirkendall shift may be suppressed, and Kirkendall voiding is observed in its pure form [6–8].

The inverse Kirkendall effect refers to cases where an existing vacancy flux (generated by some external forces) affects the interdiffusion of A and B. A classic example is irradiation, under which segregation in a homogeneous AB alloy occurs because the irradiation has produced excess vacancies and a flux of vacancies. Another example is a homogeneous AB alloy with a hollow shell structure in nanoscale [6–12], as shown in Fig. 1a. When such a hollow

* Corresponding author. Tel.: +380 472 371220.
E-mail addresses: gusak@cdu.edu.ua, gusak@routec.net (A.M. Gusak).

1359-6454/$36.00 © 2009 Acta Materialia Inc. Published by Elsevier Ltd. All rights reserved.
doi:10.1016/j.actamat.2009.03.043

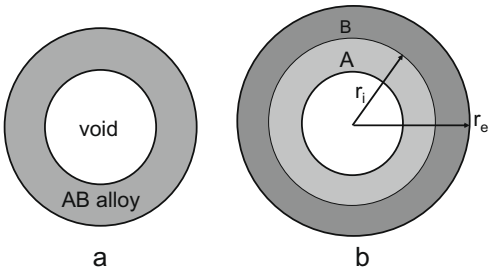

Fig. 1. Hollow nanoshell consisting of (a) initially homogeneous alloy or (b) two shells. In case (a), segregation may hinder shrinking. In case (b), the vacancy gradient between the inner and outer boundaries changes the interdiffusion kinetics.

nanoshell of a homogeneous alloy is annealed at constant temperature, de-alloying or segregation of A and B occurs [10]. This is different from thermomigration or the Soret effect, which occurs in temperature gradient. The segregation in nanoshell takes place isothermally. This is due to the Gibbs–Thomson effect, as there will be a higher vacancy concentration near the inner shell surface than that near the outer shell surface. Because of the vacancy concentration gradient, the vacancy flux is induced, and the hollow shell is unstable, and this leads to de-alloying or segregation. The faster diffusing species will segregate to the inner shell and create a gradient of chemical potential which will retard the vacancy flux. Provided the vacancy potential is larger than the counter potential of de-alloying, the hollow shell may transform to a solid sphere in order to reduce the total surface area.

Thus, when one considers the interdiffusion of A and B in a two-layer nano-shell structure, as shown in Fig. 1b, the Kirkendall effect and the inverse Kirkendall effect coexist, but how they interact with each other is not completely clear. If the flux of A, J_A, is bigger than the flux of B, J_B, the balancing vacancy flux J_V will diffuse inward, which will counter the vacancy flux due to Gibbs–Thomson effect. Conversely, if $J_A < J_B$, the two vacancy fluxes will move in the same direction, outwards. In this paper, the term "Kirkendall effect" is used to include both Kirkendall shift and Kirkendall voiding (or Frenkel voiding). A detailed analysis of the interaction of the Kirkendall effect and the inverse Kirkendall effect in nanoscale particles is presented. The interaction is expressed in terms of the interaction of vacancy fluxes, namely the difference arising between vacancy concentrations at the inner and external boundaries (higher at inner boundary and lower at the external one) should oppose the vacancy flux generated by the difference in mobilities of the main components at interdiffusion. Therefore, one expects that, under critical conditions, void formation in the hollow nanoshell can be suppressed.

2. Kinetic analysis

Consider, for example, the formation of cobalt sulfide (Co_9S_8 transforming to Co_3S_4) hollow nanospheres [6,8], as shown in Fig. 2. Because Co is the dominant diffusing species in cobalt sulfide, the voids form in the inner part of the sphere, between the remaining Co core and the growing sulfide shell. The following simplified geometry of the intermediate stages of reaction has been observed experimentally [8]: the remaining metallic core inside, surrounded by an "almost hollow" layer, contains "bridges" connecting the core and the sulfide layer. The bridges provide paths for metal atoms to diffuse and react with sulfur in the growing sulfide nanoshell. This picture is very close to the model of a so-called divided (separated) diffusion couple, which was proposed by one of the authors (AG) [13,14]. In this model the diffusion contact between powders of different materials is maintained by surface diffusion and sometimes by vapor phase transfer.

This paper is restricted to the formation of a single compound. Competition and sequential growth of phases will be analyzed elsewhere. Let r_i and r_e be the radii of inner and outer boundaries of the sulfide layer, respectively.

The following assumptions will be made in the analysis of interdiffusion in forming the nanoshells. (1) There is no Kirkendall shift during phase formation, i.e., all vacancy fluxes go to the formation of Kirkendall (or Frenkel) voids instead of being annihilated by internal sinks, hence without causing the lattice shift. (2) At the intermediate stage (after nucleation of several initial voids), the voids surround the remaining metallic core, which is connected to the growing sulfide spherical layer by a few thin bridges, as shown at Fig. 2. This means that the inner surface of the growing compound shell is mostly free but provided with very good diffusion contact with the remaining core by surface diffusion along the bridges. (3) No internal stress is involved. (4) Spherically symmetrical geometry is used. (5) The surface tensions of the external and internal boundaries of the growing phase are assumed to be identical (for the sake of simplicity).

The Laplace tension and compression of the sulfide layer due to the curvatures of the inner and outer interfaces will be taken into account in the analysis. However, vacancy super-saturation is assumed to be outside the sulfide layer (in the Co core) at the initial stage of the reaction, so voids can be nucleated. The curvature effect on vacancy concentration exists, so the difference in vacancy concentrations at the inner and external boundaries of the sulfide cannot be neglected. On the basis of the Gibbs–Thomson effect, the equilibrium vacancy concentration at the inner

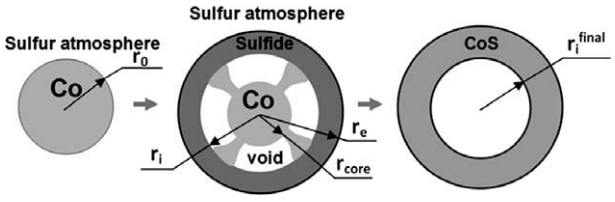

Fig. 2. Simplified scheme of sulfide nano-shell formation. At the intermediate stage, the remaining metallic core is connected to the growing compound shell by "bridges". This geometry appears as a result of the formation of voids at the interface at the initial stage of the reaction.

boundary of the sulfide layer is higher than that at the flat free surface ($c_V(r_i) = c_{V_0} e^{\frac{2\gamma\Omega}{kTr_i}}$) and, at the outer boundary, it is lower than that at the flat surface ($c_V(r_e) = c_{V_0} e^{-\frac{2\gamma\Omega}{kTr_e}}$). Thus, a vacancy gradient exists in the sulfide layer. The effect of curvature on the driving force of sulfide formation (and, respectively, on the homogeneity range of sulfide) is also included.

2.1. A simple case of the competition between "Kirkendall-driven" and "curvature-driven" effects

Starting with a simplified situation, the initial stage of compound nano-shell formation, when the shell thickness $r_e - r_i$ is much less than the initial particles radius r_0, is considered. In this case, one can use the flux equation for planar interfaces. Moreover, let the curvature effect be linear: $\frac{2\gamma\Omega}{kTr_0} \ll 1$, so that

$$\begin{cases} c_V(r_e) = c_{V_0} e^{-\frac{2\gamma\Omega}{kTr_e}} \simeq c_{V_0} \cdot \left(1 - \frac{2\gamma\Omega}{kTr_e}\right) \\ c_V(r_i) = c_{V_0} e^{\frac{2\gamma\Omega}{kTr_i}} \simeq c_{V_0} \cdot \left(1 + \frac{2\gamma\Omega}{kTr_i}\right) \end{cases} \tag{1}$$

Then the product of the vacancy flux density and the atomic volume (Ω) is determined by a simple equation, taking into account the vacancy concentration gradient caused by the Gibbs–Thomson effect:

$$\begin{aligned} \Omega j_V &= (D_m - D_S)\frac{c_m(r_e) - c_m(r_i)}{\Delta r} - D_V \frac{c_V(r_e) - c_V(r_i)}{\Delta r} \\ &\approx -(D_m - D_S)\frac{\Delta c_m}{\Delta r} + D_V c_{V_0} \cdot \frac{2\gamma\Omega}{kT}\left(\frac{1}{r_i} + \frac{1}{r_e}\right)\frac{1}{\Delta r} \end{aligned} \tag{2}$$

Here, $D_m = D_m^* \varphi, D_S = D_S^* \varphi$, where the thermodynamic factor $\varphi = \frac{c_m c_S}{kT}\frac{\partial^2 g}{\partial c_m^2}$, and D_m^*, D_S^* are tracer diffusivities of the metal and sulfur in the sulfide, respectively. Eq. (2) has taken $c_m D_m^* + c_S D_S^* = c_V D_V$. (Thus, a correlation factor is neglected here.)

Furthermore, $\Delta c_m = c_m(r_i) - c_m(r_e)$ is the homogeneity range of the compound (typically very narrow). Note that the concentration of metal and sulfur, c_m and c_s, respectively, are mole fractions, so $c_m + c_s = 1$, and $1/\Omega$ is the number of atoms per unit volume.

The first term on the right-hand side of Eq. (2) is an inward vacancy flux caused by the difference in diffusivities and leading to void formation. The second term in the same equation is an outward vacancy flux caused by different signs of curvature at the inner and outer boundaries and counteracting the first term. After all the metal is consumed, this vacancy concentration difference leads to collapse of the nanoshell. Evidently, if the curvature effect wins, meaning

$$(D_m - D_S)\frac{\Delta c_m}{\Delta r} < D_V c_{V_0} \cdot \frac{2\gamma\Omega}{kT}\left(\frac{1}{r_i} + \frac{1}{r_e}\right)\frac{1}{\Delta r} \tag{3}$$

void formation becomes impossible, because the vacancy flux should be directed outwards. At the initial stage, when $r_e \approx r_i \approx r_0$, this criterion can be rewritten as

$$r_0 < \frac{2\gamma\Omega}{kT} \cdot \frac{2(c_m D_m^* + c_S D_S^*)}{(D_m - D_S)\Delta c_m} \tag{3a}$$

The criterion in Eq. (3a) is hard to use, because the homogeneity range of the compound is very narrow and usually unknown. Yet, this difficulty can be easily circumvented. Indeed, take

$$\begin{aligned} D_m \Delta c_m &= \int_{c_m(r_e)}^{c_m(r_i)} D_m^* \varphi dc_m = \int_{c_m(r_e)}^{c_m(r_i)} D_m^* \frac{c_m c_S}{kT}\frac{\partial^2 g}{\partial c_m^2} dc_m \\ &\simeq \bar{D}_m^* \frac{\bar{c}_m \bar{c}_S}{kT} \int_{c_m(r_e)}^{c_m(r_i)} \frac{\partial^2 g}{\partial c_m^2} dc_m \\ &= \bar{D}_m^* \frac{\bar{c}_m \bar{c}_S}{kT} \cdot \left(\left.\frac{\partial g}{\partial c_m}\right|_{r_i} - \left.\frac{\partial g}{\partial c_m}\right|_{r_e}\right) = \bar{D}_m^* \frac{\Delta g}{kT} \end{aligned} \tag{4}$$

Here Δg is the compound formation Gibbs free energy per atom (it has been measured for many compounds). As a result, Eq. (4) can be reduced to the following form:

$$r_0 < \frac{2\gamma\Omega}{\Delta g} \cdot 2c_m \cdot \frac{((D_m^*/D_S^*) + c_S/c_m)}{((D_m^*/D_S^*) - 1)} \tag{5}$$

The non-dimensional parameter $G = \frac{2\gamma\Omega}{\Delta g r_o}$ is used as a measure of the ratio of the curvature effect to the chemical driving force of the reaction. Thus, in this simplified approach, the condition of impossibility for a hollow shell to form by the reaction can be represented as

$$G > \frac{1}{2c_m} \cdot \frac{(D_m^*/D_S^*) - 1}{(D_m^*/D_S^*) + c_S/c_m} \tag{6}$$

This simplified analysis neglects the influence of curvature on the chemical driving force (in other words, on the homogeneity range of the main components), and the non-linearity of the Gibbs–Thomson effect for vacancy concentration at nanoscale, spherical geometry. Moreover, knowledge of the vacancy flux is not sufficient to predict the reaction rate and the resulting void size. All this will be modified below. Nevertheless, the simplified Eq. (6) is relatively close to the graphical criterion obtained by a more rigorous analytical and numerical analysis (presented in Fig. 5).

2.2. General case

One starts from the flux balance for metal at the outer boundary and the flux balance for sulfur at the inner boundary. Flux balance means that the product of the concentration step across the boundary and the boundary velocity is equal to the difference in fluxes on both sides of this moving boundary. For the external boundary, the flux balance for metal is more convenient, because one knows for sure that both the concentration of the metal and the outward flux of the metal are equal to zero. However, for the internal boundary, the flux balance of sulfur is more convenient, because one knows almost certainly that the solubility of sulfur in the metal can be neglected, and no sulfur goes into the void, so that the corresponding

concentration and flux of sulfur at $r < r_i$ are equal to zero. Thus, each flux balance equation will use only one flux (metal for the external and sulfur for the inner boundary).

The expression for both fluxes (Eq. (7a) and (7b)) takes into account the input of vacancy gradients due to the Gibbs–Thomson effect (the last term in Eqs. (7a) and (7b)) [10]. Note that the diffusion of the metal flux is directed out of the shell; the diffusion of the sulfur flux is directed into it.

At the external radius r_e, one has

$$(0 - c_m)\frac{dr_e}{dt} = 0 - \left(-D_m\frac{\partial c_m}{\partial r}\bigg|_{r_e} + \frac{c_m D_m^*}{c_V}\frac{\partial c_V}{\partial r}\bigg|_{r_e}\right) \tag{7a}$$

At the internal radius r_i, one has

$$(c_S - 0)\frac{dr_i}{dt} = \left(-D_S\frac{\partial c_S}{\partial r}\bigg|_{r_i} + \frac{c_S D_S^*}{c_V}\frac{\partial c_V}{\partial r}\bigg|_{r_i}\right) - 0 \tag{7b}$$

Concentrations of metal and sulfur inside the sulfide can change slightly in the narrow homogeneity ranges for the atomic fractions of metal and sulfur inside the sulfide, respectively ($\Delta c_m = -\Delta c_S$). Consider that

$$c_m + c_S \cong 1, \quad \frac{\partial c_S}{\partial r} \cong -\frac{\partial c_m}{\partial r}$$

Note that the fluxes in the lattice reference frame and intrinsic diffusivities (instead of interdiffusivity) are used according to the basic approximation of no Kirkendall shift. The correlation factors of Manning's vacancy wind terms [15] are neglected, as they can change the results only quantitatively. Both tracer diffusivities are proportional to the vacancy concentration. (Here, one more approximation is used that only one effective vacancy concentration is treated, without distinguishing between sublattices in the sulfide.) Take

$$D_m^* = c_V * K_m, \quad D_S^* = c_V * K_S \tag{8}$$

where K_m and K_S can be treated as constants. Thus, Eq. (7a) and (7b) is rearranged as

$$\frac{dr_e}{dt} = K_m \cdot \left(-\frac{c_V\varphi}{c_m}\frac{\partial c_m}{\partial r}\bigg|_{r_e} + \frac{\partial c_V}{\partial r}\bigg|_{r_e}\right) \tag{9a}$$

$$\frac{dr_i}{dt} = K_S \cdot \left(\frac{c_V\varphi}{c_S}\frac{\partial c_m}{\partial r}\bigg|_{r_e} + \frac{\partial c_V}{\partial r}\bigg|_{r_e}\right) \tag{9b}$$

Note that, in the above equations, the values of vacancy concentration at the external and internal boundaries can be very different, owing to the Gibbs–Thomson effect, and the vacancy gradient (and the cross-terms in Eqs. (7) and (10)) do not tend to zero. At the same time, the concentrations of the main components at the external and internal boundaries remain close to constant because of the narrow homogeneity range of the sulfide.

Now, a steady-state approximation is used for both components and vacancies inside the sulfide, which has proved to be valid inside intermediate phases with a narrow homogeneity range [16]. From the continuity equation, one has

$$\frac{\partial c_m}{\partial t} \approx 0 \Rightarrow div\vec{J}_m \approx 0, \quad \frac{\partial c_V}{\partial t} = div\vec{J}_V + \sigma_V \approx div\vec{J}_V \approx 0 \Rightarrow div\vec{J}_V \approx 0 \tag{10}$$

In the last equation, the assumption about the absence of effective vacancy sinks/sources inside the growing layer of sulfide was used.

Writing down the fluxes and divergences in spherical coordinates, one obtains

$$div\vec{j} \approx 0 \Rightarrow \frac{1}{r^2}\frac{\partial}{\partial r}(r^2 j_r) \approx 0 \Rightarrow r^2 j_r \approx const$$

$$r^2 \cdot \Omega j_m(r) = r^2\left(-c_V(r)\varphi\frac{\partial c_m}{\partial r} + c_m(r)\frac{\partial c_V}{\partial r}\right)K_m = r_e^2 \cdot \Omega j_m(r_e) = r_e^2 \cdot \frac{dr_e}{dt} \cdot c_m \tag{11}$$

$$r^2 \cdot \Omega j_S(r) = r^2\left(-c_V(r)\varphi\frac{\partial c_S}{\partial r} + c_S(r)\frac{\partial c_V}{\partial r}\right)K_S = r_i^2 \cdot \Omega j_S(r_i) = r_i^2 \cdot \frac{dr_i}{dt} \cdot c_S \tag{12}$$

where $\Omega j_{\mathrm{m}} = c_{\mathrm{m}}\frac{dr_e}{dt}$ and $\Omega j_{\mathrm{S}} = c_{\mathrm{S}}\frac{d_i}{dt}$ are fluxes of the metal and sulfur, respectively, and Ω is the volume per atom of the sulfide.

Eqs. (11) and (12) can be treated as the set of two differential equations for two unknown functions $c_m(r), c_V(r)$ (treating r_e and r_i and their time derivatives as known parameters). These equations are non-linear because the vacancy concentration $c_V(r)$ and thermodynamic factor $\varphi(r)$ in the coefficients cannot be treated as constants. However, Eqs. (11) and (12) can be treated as the linear set of *algebraic* equations for determining $\frac{dc_V}{dr}$ and $c_V(r)\varphi(r)\frac{dc_m}{dr}$. By rearrangement, Eqs. (11) and (12) are changed to

$$\begin{cases} \frac{dc_V}{dr} = \frac{B_2}{r^2} \\ c_V(r)\varphi(r)\frac{dc_m}{dr} = -\frac{B_1}{r^2} \end{cases} \tag{13}$$

where B_1 and B_2 are expressed in terms of the boundary velocities

$$\begin{cases} B_2 = -\frac{c_S}{K_S}r_i^2\frac{dr_i}{dt} - \frac{c_m}{K_m}r_e^2\frac{dr_e}{dt} \\ B_1 = c_m c_S \cdot \left(\frac{r_e^2}{K_m}\frac{dr_e}{dt} - \frac{r_i^2}{K_S}\frac{dr_i}{dt}\right) \end{cases} \tag{14}$$

The solutions of Eq. (13) give

$$\begin{cases} c_V(r) = -\frac{B_2}{r} + F \\ \varphi\frac{dc_m}{dr} = \frac{B_1}{r^2\left(-\frac{B_2}{r}+F\right)} \end{cases} \tag{15}$$

where F is the integration constant. In the first equation in Eq. (15), the boundary conditions at r_e and r_i, taking into account the Gibbs–Thomson effect on the vacancy concentration, will give

$$\begin{cases} c_V(r_e) = -\frac{B_2}{r_e} + F = c_{V_0}e^{-\frac{2\gamma\Omega}{kTr_e}} \\ c_V(r_i) = -\frac{B_2}{r_i} + F = c_{V_0}e^{\frac{2\gamma\Omega}{kTr_i}} \end{cases} \tag{16}$$

Then, the second equation in Eq. (15) is integrated over the radius from the inner boundary to the outer one, giving

$$\int_{r_i}^{r_e}\varphi\frac{dc_m}{dr}dr=\int_{r_i}^{r_e}\frac{B_1}{r^2\left(-\frac{B_2}{r}+F\right)}dr \tag{17}$$

The integration of the right-hand side of Eq. (17) by substituting Eq. (16) gives

$$\frac{B_1}{B_2}\int_{r_i}^{r_e}\frac{d\left(-\frac{B_2}{r}+F\right)}{\left(-\frac{B_2}{r}+F\right)}=\frac{B_1}{B_2}\int_{c_V(r_i)}^{c_V(r_e)}\frac{dc_V}{c_V}=\frac{B_1}{B_2}\cdot\left(\ln\frac{c_V(r_e)}{c_V(r_i)}\right)=-\frac{B_1}{B_2}\frac{2\gamma\Omega}{kT}\left(\frac{1}{r_e}+\frac{1}{r_i}\right) \tag{18}$$

For the integration of the left-hand side of Eq. (17), taking into account that the thermodynamic factor $\varphi=\frac{c_mc_S}{kT}\frac{\partial^2 g}{\partial c_m^2}$, and that the homogeneity interval is very narrow (concentrations are almost constant within the sulfide layer, but the derivatives of g are very far from being constant), one obtains

$$\int_{r_i}^{r_e}\varphi\frac{dc_m}{dr}dr=\int_{r_i}^{r_e}\frac{c_mc_S}{kT}\frac{\partial^2 g}{\partial c_m^2}\frac{dc_m}{dr}dr=\frac{\bar{c}_m\bar{c}_S}{kT}\int_{c_m(r_i)}^{c_m(r_e)}\frac{\partial^2 g}{\partial c_m^2}dc_m=\frac{\bar{c}_m\bar{c}_S}{kT}\cdot\left(\left.\frac{\partial g}{\partial c_m}\right|_{r_e}-\left.\frac{\partial g}{\partial c_m}\right|_{r_i}\right) \tag{19}$$

It is well known for the case of planar layer growth that, for the growth of a single intermediate phase, the difference in the right and left derivatives would be proportional to the driving force of the reaction

$$\left.\frac{\partial g}{\partial c_m}\right|_{r_e}-\left.\frac{\partial g}{\partial c_m}\right|_{r_i}=\left.\frac{\partial g}{\partial c_m}\right|_{\infty}^{compound/nonmetal}-\left.\frac{\partial g}{\partial c_m}\right|_{\infty}^{compound/metal}=-\frac{\Delta g}{\bar{c}_m\bar{c}_S} \tag{20}$$

Yet, in the present case, one should take into account the influence of curvature not only on the vacancy concentration, but also on the phase equilibrium at the curved boundaries. At the external boundary, the sulfide is under additional Laplace compression with additional energy per atom $\frac{2\gamma\Omega}{r_e}$, so that, taking into account the common tangent rule, one has

$$\left.\frac{\partial g}{\partial c_m}\right|_{r_e}=\left.\frac{\partial g}{\partial c_m}\right|_{\infty}^{compound/nonmetal}+\frac{\frac{2\gamma\Omega}{r_e}}{c_m(r_e)-0}\cong\left.\frac{\partial g}{\partial c_m}\right|_{\infty}^{compound/nonmetal}+\frac{2\gamma\Omega}{\bar{c}_mr_e} \tag{21}$$

At the internal boundary, the sulfide shell is under Laplace tension with negative additional energy per atom $\left(-\frac{2\gamma\Omega}{r_i}\right)$, so that

$$\left.\frac{\partial g}{\partial c_m}\right|_{r_i}=\left.\frac{\partial g}{\partial c_m}\right|_{\infty}^{compound/metal}+\frac{-\frac{2\gamma\Omega}{r_i}}{c_m(r_i)-1}\cong\left.\frac{\partial g}{\partial c_m}\right|_{\infty}^{compound/metal}+\frac{2\gamma\Omega}{\bar{c}_Sr_e} \tag{22}$$

Then, instead of Eq. (20), one obtains

$$\left.\frac{\partial g}{\partial c_m}\right|_{r_e}-\left.\frac{\partial g}{\partial c_m}\right|_{r_i}=-\frac{\Delta g}{\bar{c}_m\bar{c}_S}+\frac{2\gamma\Omega}{\bar{c}_mr_e}-\frac{2\gamma\Omega}{\bar{c}_Sr_i} \tag{23}$$

Substituting Eq. (23) into Eq. (19), one obtains

$$\int_{r_i}^{r_e}\varphi\frac{dc_m}{dr}dr=\frac{\bar{c}_m\bar{c}_S}{kT}\cdot\left(\left.\frac{\partial g}{\partial c_m}\right|_{r_e}-\left.\frac{\partial g}{\partial c_m}\right|_{r_i}\right)=-\frac{\Delta g}{kT}+\frac{2\gamma\Omega}{kT}\left(\frac{\bar{c}_S}{r_e}-\frac{\bar{c}_m}{r_i}\right) \tag{24}$$

It is interesting to note that the change in driving force in Eq. (24) due to curvature effect can be negative as well as positive, depending on the stoichiometry and on the ratio of the external and internal radii.

Substituting Eqs. (24) and (18) into Eq. (17), one obtains

$$\frac{\Delta g}{2\gamma\Omega}-\frac{\bar{c}_S}{r_e}+\frac{\bar{c}_m}{r_i}=\frac{B_1}{B_2}\cdot\left(\frac{1}{r_e}+\frac{1}{r_i}\right) \tag{25}$$

After substituting B_1 and B_2 from Eq. (14) into Eq. (25) and after excluding the time, one obtains (after simple but long algebra) the main equation of this paper:

$$\frac{dr_e}{dr_i}=-\frac{r_i^2}{r_e^2}\frac{K_m}{K_S}\frac{c_S}{c_m}\frac{\frac{\Delta g}{2\gamma\Omega}-\frac{1}{r_e}}{\frac{\Delta g}{2\gamma\Omega}+\frac{1}{r_i}} \tag{26}$$

The following non-dimensional parameters are used:

$x=\frac{r_i}{r_o}, y=\frac{r_e}{r_o}, G=\frac{2\gamma\Omega}{\Delta gr_o}$, where r_o is the initial radius of the nanoparticle. The "G parameter" G, together with the ratio of mobilities $\frac{K_m}{K_S}=\frac{D_m^*}{D_S^*}=\frac{D_m}{D_S}(D_{m(S)}=D_{m(S)}^*\varphi)$ are the two major parameters of the model. Eq. (26) can then be represented in the following form:

$$\frac{dy}{dx}=-\frac{x^3}{y^3}\frac{D_m^*}{D_S^*}\frac{1-c_m}{c_m}\frac{y-G}{x+G} \tag{27}$$

This equation differs from a similar equation by Alivisatos et al. [8] by the last term containing $G\neq 0$ (responsible for the Laplace pressure and the Gibbs–Thomson effect for both vacancies and main components). When both radii r_e and r_i are large $\left(r_e,r_i\gg\frac{2\gamma\Omega}{\Delta g}, G\ll 1\right)$, the equations become similar.

Eq. (29) can be easily integrated but gives, as a result, the transcendent interrelation between y and x. It can be solved numerically by the finite difference method. The governing parameters are: $D\equiv\frac{D_m^*}{D_S^*}, c_m$ and G. The equation has been solved with the "initial" condition $x=1, y=1+\varepsilon$. Calculations were made in two cases: (1) when all pure metal (core) was consumed by reaction

$$c_m\cdot(y^3-x^3)\geqslant 1 \tag{28}$$

and (2) when the inner radius of the sulfide shell became equal to the radius of the remaining metallic core (the void in the hollow shell between the compound shell and the remaining metallic core with connecting bridges shrinks prior to the end of the reaction):

$$x^3\leqslant\frac{r_{core}^3}{r_0^3}=1-c_m\cdot(y^3-x^3) \tag{29}$$

It is evident from Eq. (27) that, in the case G > 1, nanoshell formation is impossible (taking into account that x and y start from almost 1). This means that, in very small

particles, $r_o < \frac{2\gamma\Omega}{\Delta g}$, the reaction with void formation is impossible. It is interesting that this critical condition coincides with the critical radius for nucleation of a new phase.

3. Applications of kinetic analysis

Below are presented some results for various parameters in Eq. (27). A characteristic solution of Eq. (27) is represented in Fig. 3. Here the reduced inner radius x was decremented uniformly and arbitrarily, the reduced external radius y was calculated by numerical integration of Eq. (27), and the reduced radius $z = r_{core}/r_0$ of the remaining core was calculated according to conservation of matter (neglecting the difference in atomic volumes in the compound and the metal): $z = (1 - c_m \cdot (y^3 - x^3))^{1/3}$. Calculations were stopped when the core or void disappeared ($z = 0$ or $x = z$).

According to the analysis by Alivisatos et al. [8], the resulting radius of the final void is determined only by the ratio of diffusivities and by the stoichiometry of the compound. (Ideally, if only metallic atoms migrate, the final void radius should be just equal to the initial radius of the metallic particle.) But, according to the present model, the resulting ratio of void radius to initial particle size depends on the initial particle size via the G factor. Indeed, according to the present results, the smaller the initial radius and the larger factor G, the lower will be the ratio of final void size to initial particle size, as shown in Fig. 4. Thus, if the initial radius is less than some critical one, voids cannot be formed at all.

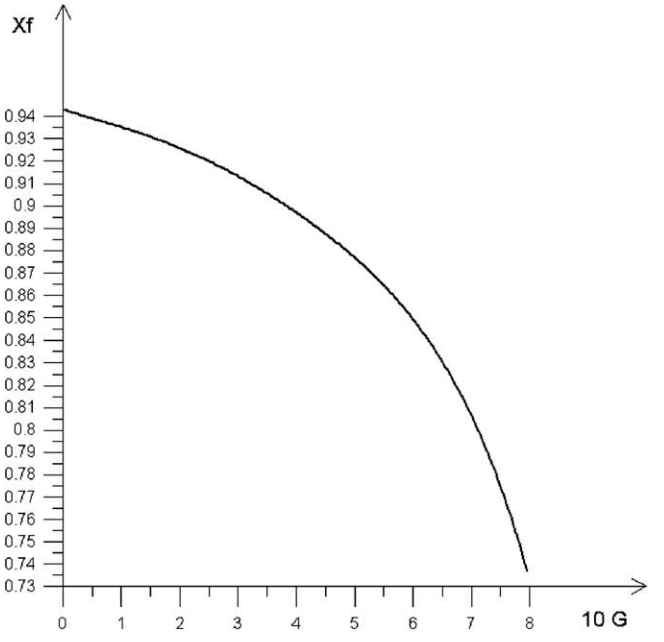

Fig. 4. Dependence of resulting reduced void radius $xf = \frac{r_i^{final}}{r_o}$ on the G parameter $\left(G = \frac{2\gamma\Omega}{\Delta g r_o}\right)$ at $D \equiv \frac{D_m^*}{D_S^*} = 10, c_m = c_S = 0.5$.

And what then? In this case, owing to the large vacancy gradient, the inner radius converges inside faster than the radius of the remaining metallic core, and abolishes the void. In Fig. 5, the region of parameters G and D $\left(G = \frac{2\gamma\Omega}{\Delta g r_o}, D \equiv \frac{D_m^*}{D_S^*}\right)$ is divided into two subregions (results of numerical calculations of $y(x)$ with various parameters of G and D). For the left and upper subregions, the forma-

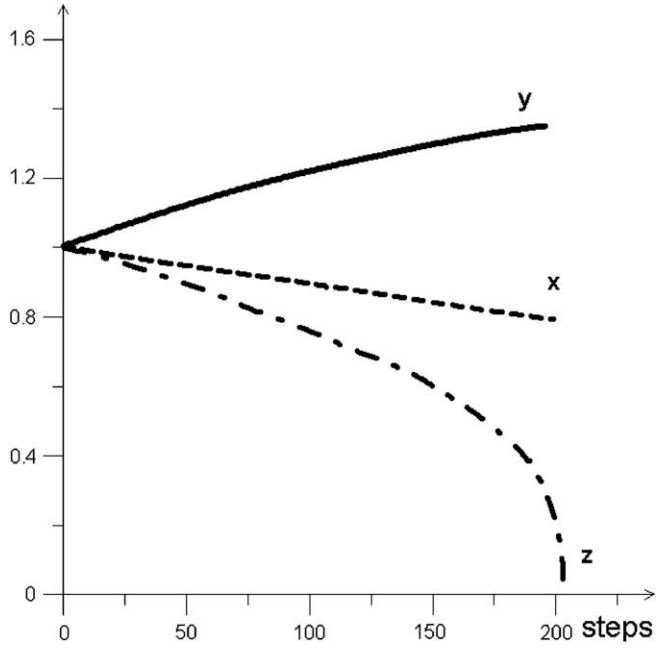

Fig. 3. Evolution of the reduced external radius $y = \frac{r_E}{r_o}$ of a compound nanoshell (solid line) and reduced radius $z = r_{core}/r_0$ of the remaining metallic core (chain line) with decreasing reduced inner radius of the nanoshell $x = \frac{r_i}{r_o}$ (dashed line). The moment of disappearance of the core corresponds to the final radius of the void (end of chain line).

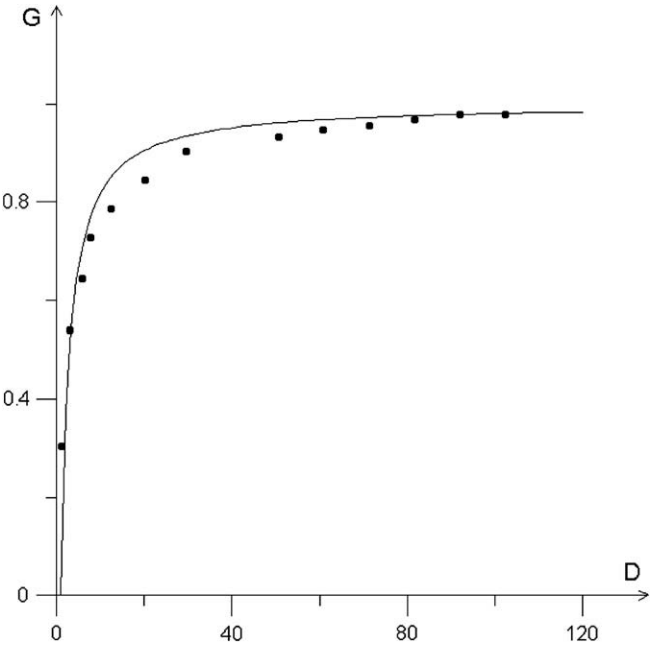

Fig. 5. Dependence $G(D)$ dividing two regimes: left and up, hollow nanoshell formation impossible. Solid line, approximate analytical criterion $G > \frac{(D_m^*/D_S^*)-1}{(D_m^*/D_S^*)+1}$ (Eq. (6) at $c_S = c_m = 1/2$). Points, numerical criterion obtained by solution of Eq. (27) with condition (29).

tion of a hollow nanoshell is forbidden. This criterion appears to be relatively close to the approximate analytical criterion in Eq. (6), as demonstrated in Fig. 5.

If necessary, one can also calculate the absolute rate of void formation in real time. Indeed, one can deduce two expressions for parameter B_2. First, from the set of Eqs. (16), one obtains

$$B_2 = -c_{V_0}\frac{e^{\frac{2\gamma\Omega}{kTr_i}} - e^{-\frac{2\gamma\Omega}{kTr_e}}}{\frac{1}{r_i} - \frac{1}{r_e}} \tag{30}$$

Second, from Eqs. (14) and (26), one obtains:

$$B_2 = -\frac{c_S}{K_S} r_i^2 \frac{dr_i}{dt} - \frac{c_m}{K_m} r_e^2 \frac{dr_e}{dt} = -\frac{c_S}{K_S} r_i^2 \frac{dr_i}{dt} \cdot \left(1 - \frac{r_i}{r_e}\frac{\frac{r_e}{r_0} - G}{\frac{r_i}{r_0} + G}\right) \tag{31}$$

Equalizing (30) and (31) gives

$$\frac{dr_i}{dt} = -\frac{K_S c_{V0}}{c_S}\frac{\exp\left(\frac{2\gamma\Omega}{kTr_i}\right) - \exp\left(-\frac{2\gamma\Omega}{kTr_e}\right)}{r_i^2\left(\frac{1}{r_i} - \frac{1}{r_e}\right)\left(1 - \frac{r_i}{r_e}\frac{r_e/r_0 - G}{r_i/r_0 + G}\right)} \tag{32}$$

Combining Eqs. (26), (27) with Eq. (32) gives the full description of the kinetics in real time. A typical result of solving Eq. (32) together with the Eq. (27) is shown in Fig. 6.

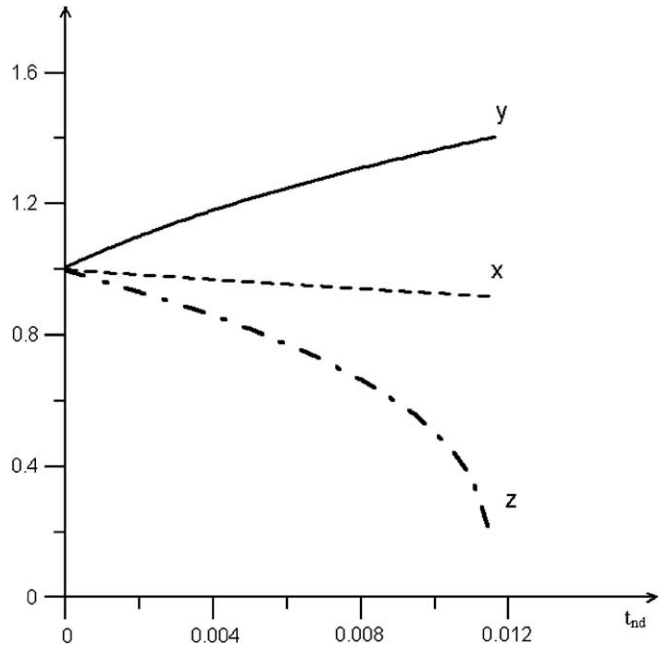

Fig. 6. Dependence of reduced external ($y = r_e/r_0$), internal radii ($x = r_i/r_0$) of the nanoshell and remaining core radius ($z = r_{core}/r_0 = (1 - c_m \cdot (y^3 - x^3))^{1/3}$) on non-dimensional time $t_{nd} = \frac{D_S^*}{r_0^2}t$, calculated according to Eq. (32). Case $D \equiv \frac{D_m^*}{D_S^*} = 10, c_m = c_S = 0.5, \frac{2\gamma\Omega}{kTr_0} = 1$.

4. Conclusion

The formation of a hollow nanoshell was analyzed by three competing factors: (1) growth of the compound phase owing to the reaction and tendency for vacancies to go inside (due to difference in diffusivities); (2) shrinking of the shell owing to the vacancy gradient between the inner and outer boundaries (the Gibbs–Thomson effect); and (3) change in the driving force by Laplace tension at the inner boundary and Laplace compression at the external boundary. The second factor should win for very small particles. The critical value for the initial radius is very similar to the Gibbs nucleation theory, that is $r_0^{cr} = \frac{2\gamma\Omega}{\Delta g}$. Nucleation and phase competition (in case of two phase sequential formation) of the spherical particles will be considered elsewhere in the lines of [17].

Acknowledgements

The author (AMG) acknowledges the support of the Ukrainian Ministry of Education and Science, and of the State Foundation for Fundamental Research (Ukraine), Grant Φ25.4/162. The author (KNT) acknowledges support from NSF/NIRT Contract # 0506841. The authors would like to thank Dmytro Kovalenko and Sergiy Voroshnin at ChNU for checking equations, and Miss Di Xu at UCLA for the drawing the figures.

References

[1] Smigelkas AD, Kirkendall EO. Trans AIME 1947;171:130.
[2] Darken LS. Trans AIME 1948;175:184.
[3] Geguzin YE. Diffusion zone. Moscow: Nauka; 1979 (in Russian).
[4] Hoglund L, Agren J. Acta Mater 2001;49:1311.
[5] Strandlund H, Larsson H. Acta Mater 2004;52:4695.
[6] Yin Y, Rioux RM, Erdonmez CK, Hughes S, Somorjai GA, Alivisatos P. Science 2004;304:711.
[7] Wang CM, Baer DR, Thomas LE, Amonette JE, Anthony J, Qiang Y, et al. Appl Phys 2005;98:094308.
[8] Yin Y, Erdonmez CK, Cabot A, Hughes S, Alivisatos AP. Adv Funct Mater 2006;16:1389.
[9] Tu KN, Gosele U. Appl Phys Lett 2005;86:093111.
[10] Gusak AM, Zaporozhets TV, Tu KN, Goesele U. Philos Mag 2005;85:4445.
[11] Evteev AV, Levchenko EV, Belova IV, Murch GE. Philos Mag 2007;87:3787.
[12] Evteev AV, Levchenko EV, Belova IV, Murch GE. Def Diff Forum 2008;277:21.
[13] Gusak AM. Poroshkovaya metallurgiya (Powder metall) 1989;3:39 (in Russian).
[14] Gusak AM, Lucenko GV. Acta Mater 1998;46:3343.
[15] Manning J. Acta Metall 1967;15:817.
[16] Gusak AM, Yarmolenko MV. J Appl Phys 1993;73:4881.
[17] Hodaj F, Gusak AM, Desre PJ. Philos Mag A 1998;77:147.